

# Analysis and Design of Single-layer Lattice Aluminum Domes Using ANSYS Workbench

Wei-Ling Hsu,<sup>1</sup> Hong-Wei Yu,<sup>2</sup> Chao-Ming Hsu,<sup>2\*</sup>  
Te-Hsun Lin,<sup>3</sup> Sufen Wei,<sup>4</sup> and Cheng-Fu Yang<sup>5,6\*\*</sup>

<sup>1</sup>School of Civil Engineering, Jiaying University, Meizhou, Guangdong, 514015, China

<sup>2</sup>Department of Mechanical Engineering, National Kaohsiung University of Science and Technology, Kaohsiung 807, Taiwan

<sup>3</sup>School of Economics and Management of Jiaying University, Meizhou, Guangdong, 514015, China

<sup>4</sup>School of Ocean Information Engineering, Jimei University, Xiamen 361021, China

<sup>5</sup>Department of Chemical and Materials Engineering, National University of Kaohsiung, Kaohsiung 811, Taiwan

<sup>6</sup>Department of Aeronautical Engineering, Chaoyang University of Technology, Taichung 413, Taiwan

(Received July 15, 2023; accepted September 25, 2023)

**Keywords:** single-layer lattice aluminum dome, stress and deformation, ANSYS Workbench, uneven live load

The single-layer reticular aluminum dome has gained popularity in the fabrication industry of domes for trough roofs owing to its numerous advantages, including its lightweight nature, durability, affordability, ease of assembly and disassembly, as well as convenient maintenance. The objective of this study was to simulate and analyze domes designed on the basis of the test standards specified in the American Petroleum Institute's API Standard 650: Appendix G, which pertains to single-layer reticulated aluminum domes, and to ensure compliance with its requirements. Two types of vault were designed with varying dimensions and methods of connecting groove walls. To assess the structural integrity of the domes, finite element analysis was performed. Both vault designs were subjected to six different load combinations to determine if the material would fail owing to insufficient yield strength. The primary focus of this research is on the vault structure's design and finite element analysis. Following the compilation of design points, a three-dimensional model of the vault was created. The stress and deformation of the vault were simulated using the finite element analysis software ANSYS Workbench, considering various conditions. The stress and deformation analyses indicated that both vault designs successfully met the criteria outlined in the code.

## 1. Introduction

The single-layer mesh aluminum vault is a fixed groove roof that possesses a unique geometric structure. This structure allows for the effective and even distribution of tension throughout the entire vault. Consequently, the peripheral support beams connected to the tank wall are capable of sustaining the entire structure without the need for additional support

---

\*Corresponding author: e-mail: [yhlepp@gmail.com](mailto:yhlepp@gmail.com)

\*\*Corresponding author: e-mail: [cfyang@nuk.edu.tw](mailto:cfyang@nuk.edu.tw)

<https://doi.org/10.18494/SAM4595>

columns or reinforcements. The straightforward design of the single-layer mesh aluminum vault offers several competitive advantages. It is lightweight, durable, cost-effective, and easy to assemble and disassemble, and requires minimal maintenance. These qualities enable the use of fewer building materials and simpler manufacturing processes, resulting in significantly reduced construction costs. Hence, the single-layer mesh aluminum vault holds considerable research value, and its structure design and analysis constitute the primary focus of this research. Presently, the advancement of computer technology allows for the solution of complex nonlinear problems. Numerical analysis, which employs simulations to predict the stress and deformation of structures, has become a widely used method in this regard.

Kato *et al.* presented their findings on the impact of determining the section proportions of single-layer reticulated dome members.<sup>(1)</sup> Their approach, based on linear buckling stress, utilized a geometric stiffness matrix for precise linear buckling analysis.<sup>(1)</sup> Building upon this work, Chandiwala conducted an examination of steel domes using the computer analysis software STAAD.Pro.<sup>(2)</sup> This software provided valuable insights and analysis capabilities for studying the structural properties of the domes. Fan *et al.* proposed the Hamilton variational principle as a solution to address the current collision problem. They introduced the central difference method, an effective approach within the finite element method, to tackle collision problems and successfully solve nonlinear dynamic problems.<sup>(3)</sup> This method proved to be particularly suitable and efficient in handling complex dynamic scenarios. Fan *et al.* examined the dynamic collapse mechanism of single-layer reticulated shells subjected to harmonic loads, sudden loads, and earthquake loads.<sup>(4)</sup> Their study delved into the behavior of these structures under various loading conditions.

Nie *et al.* presented their findings on the impact of reducing the cross-sectional area of structural members. They discovered that decreasing the cross-sectional area led to reductions in plastic development and structural ductility, indicating poor performance.<sup>(5)</sup> The effects of different static preloads on counter-intuitive collapse were investigated by Ma *et al.*<sup>(6)</sup> Their research highlighted that single-story reticulated domes with significant initial collapse under dynamic loads were affected by these preloads.<sup>(6)</sup> Jihong and Nian proposed a novel numerical analysis method to explore complex mechanical behaviors, such as the large deformation of substantial or extremely large components, material nonlinearity, and fracture. Their study aimed to facilitate further investigations into these intricate phenomena.<sup>(7)</sup> Together, these advancements in structural analysis and solution methodologies have significantly contributed to the field, enabling improved understanding and practical applications in the design and analysis of reticulated dome members, steel domes, and other structural systems.

Previously, two common methods were utilized to assess the efficacy of a designed bullet-resistant door. The first method involved the application of sensors positioned at various locations to detect any cracking that occurred upon impact. For example, Nie and Liu utilized three-dimensional acceleration sensors, strategically placed at eight measuring points, to analyze the dynamic acceleration response.<sup>(8)</sup> Similarly, Zhao *et al.* utilized displacement sensors to examine the mechanical properties of a single-layer aluminum-alloy combined lattice shell structure.<sup>(9)</sup> These studies, cited as Refs. 5–9, suggest that employing simulation methods to design domes and assess their stability under different loads is a highly efficient and valid

approach. Simulation methods offer the advantage of eliminating the need for a significant financial investment in constructing physical domes. However, it is important to note that most research studies have focused on utilizing only a single variable as the simulation parameter for the designed domes. In real-world scenarios, domes are subject to multiple simultaneous loads, and only a limited number of studies have specifically investigated the effects of different loads on the stability of the designed domes. Therefore, there is a need for further research to explore the impact of various loads acting simultaneously on domes and their stability. Such investigations would provide valuable insights into the behavior and performance of domes under real-world conditions, leading to more robust and reliable designs.

The primary objective and innovative aspect of this study revolve around analyzing the effects of various loads on stress and deformation patterns within a designed dome structure. The rapid advancement of computer technology has made it possible to tackle more complex nonlinear problems through simulation methods. Numerical analysis, which involves simulating the stress state of a structure and predicting its resulting stress and deformation, has become widely employed in engineering practice. Among different dome types, single-layer reticulated aluminum domes offer numerous competitive advantages such as low weight, structural robustness, high durability, cost-effectiveness, ease of assembly and disassembly, and simplified maintenance. Therefore, in this study, we focus on simulating the behavior of single-layer reticulated aluminum domes using two different connection methods: welding and sliding bases. To conduct simulations, we utilized the FEM analysis software ANSYS Workbench.

This software enables the accurate modeling and analysis of the dome structure under various loading conditions. By comparing the results obtained from the two different connection methods, we aim to gain insights into the structural performance, stress distribution, and deformation characteristics of single-layer reticulated aluminum domes. This information is valuable for the design and optimization of such dome structures. Uematsu *et al.* conducted a seminal study on wind loads and the dynamic properties induced by wind in a long-span dome.<sup>(10)</sup> Their research focused on a rigidly connected single-layer lattice structure.<sup>(10)</sup> Building upon this work, Wang and Shen employed a Lagrangian formulation to carry out three-dimensional nonlinear analyses of beam elements.<sup>(11)</sup> Their analyses included the consideration of large rotations and displacements at joints, particularly under the effects of strong wind loads and earthquake forces.

In this study, we investigated the stability and resilience of single-layer reticulated aluminum domes by subjecting them to various load combinations. Six different load combinations were considered: static load, static load combined with uneven live load, static load combined with average live load, static load combined with wind load, static load combined with uneven live load and wind load, and static load combined with average live load and wind load. By analyzing the resulting data, which included the maximum and minimum principal stresses as well as total deformations, we aimed to assess the ability of the designed domes to withstand internal stress (static load) and external stresses (uneven live load, average live load, and wind load). Our primary focus was to prevent structure failure caused by two factors: (a) the stresses induced by external forces exceeding the yield stress of the material and (b) permanent deformations resulting from external forces.

Our findings demonstrate that, across the six different load scenarios applied to the two domes, the maximum stresses experienced were significantly lower than the maximum stress threshold of the chosen material, namely, the 6061-T6 aluminum alloy. Furthermore, the deformations observed during simulations did not result in permanent deformations. The main purpose of this study is to design single-layer lattice aluminum domes with different loads systematically and scientifically, and computer-aided engineering is used to simulate the actual structural behavior of the designed domes. After obtaining simulation analysis results, it will be possible to assess whether the designs of the single-layer lattice aluminum domes can meet specified safety standards under various specific conditions.

## 2. Simulation Process and Parameters

To ensure the structural integrity and functionality of the single-layer reticulated aluminum domes across various climates and potential environmental factors worldwide, a standard design guideline, namely, API Standard 650: Appendix G, has been established. This guideline sets forth the necessary design loads to fabricate domes with high security and resilience. In adherence to API Standard 650: Appendix G, we conducted simulation designs and structural analyses for the single-layer reticulated aluminum domes. These rigorous processes aimed to ensure the safety and security of the domes, enabling them to withstand diverse natural or man-made factors. A critical requirement specified in the standard is the maximum radius of curvature ( $R$ ) for single-layer mesh aluminum domes. It states that  $R$  should not exceed 1.2 times the diameter ( $D$ ) of the barrel tank, while the minimum  $R$  value should not be less than  $0.7 D$ . The  $R/D$  ratio directly impacts the shape and load-bearing capacity of the dome, underscoring its importance in the design process.

The designed domes had a span of 36.19 m, a ratio of the radius of curvature to the diameter of the barrel tanks set at one, and a height of 6.26 m, as shown in Fig. 1(a). In addition to these design parameters, the connection methods between the domes and the barrel tanks were of significant interest. To address this, two distinct connection methods were devised and illustrated in Figs. 1(b) and 1(c): welding base (referred to as dome 1) and sliding base (dome 2). By employing these connection methods, the aim was to compare the effects of loading on the domes' three normal stresses and maximum deformations under six different load combinations. This comparison was necessary owing to the utilization of multiple load combinations, allowing for an assessment of how the different connection methods affected the aforementioned stress and deformation characteristics of the domes.

Given the extensive application of Kaiweit-type reticulated domes in the installation and construction of storage tanks, we opted to utilize such domes as the designed structure for our simulations. However, we took into consideration that the outermost end of the reticulated shell is supported by the ring beam, resulting in a nonuniform stress distribution on the outermost ring of the Kaiweit-type structure. This uneven distribution of supports would be detrimental to the lower tank body. To address this issue, we introduced several circles of square grids, which served to distribute the bearing stress more uniformly on the ring beam. This modification aimed to improve the uneven stress distribution caused by the original design. In summary,

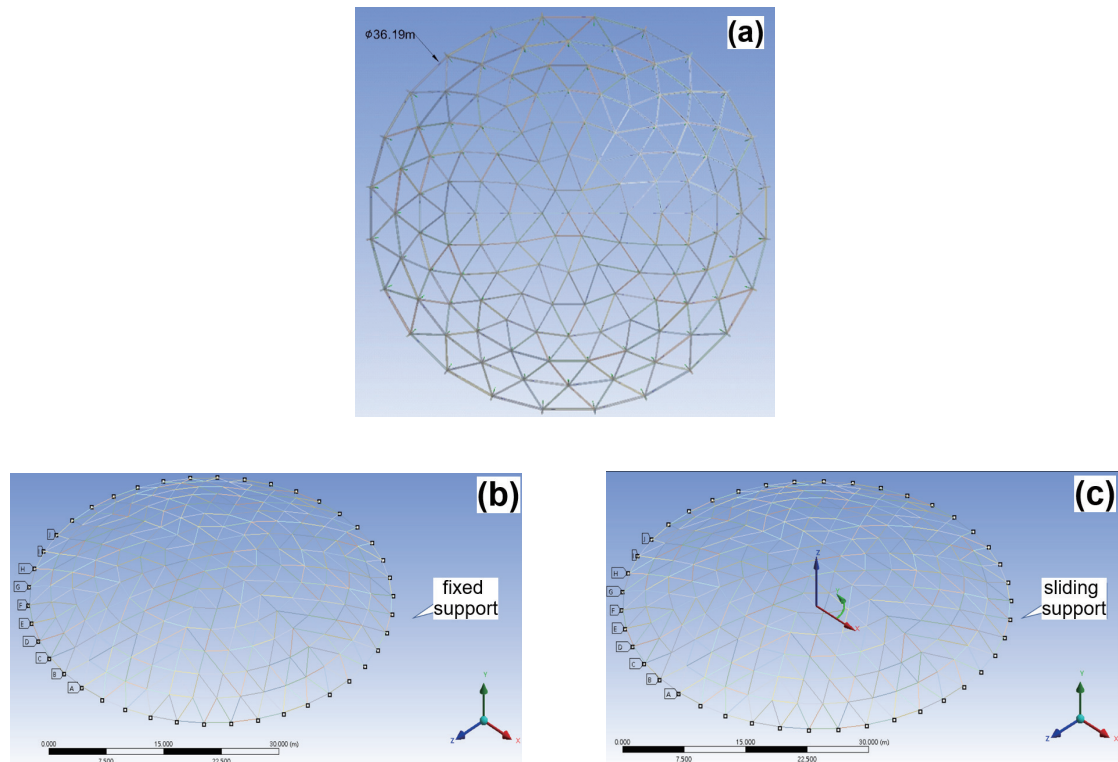


Fig. 1. (Color online) Schematic diagrams of (a) top view of the designed dome and connection method, (b) welding, and (c) sliding structures.

taking into account the structural characteristics of large-scale storage tanks, we designed mixed-type reticulated domes with a hybrid structure combining the Kaiweit-type structure and the joint-square structure. In the design of the storage tank's reticulated domes, special consideration was given to the section of rods. Unlike traditional building reticulated domes, the skins of the storage tank's domes were directly in contact with the rods.

Since the rods were subjected to bending moments, using round tubes for the rods was not suitable. Instead, I-beam members were preferred owing to their ability to withstand bending loads effectively. Furthermore, to facilitate the connections between the I-beam members, plate-type nodes were chosen over socket-type nodes. This decision was made to ensure robust and secure connections throughout the structure. As a result, the cross sections of the I-structural beams within the single-layer reticulated aluminum domes were adjusted to accommodate these plate-type connections, enabling efficient load transfer and enhanced structural integrity. These dimensions were carefully selected to meet the specific requirements of each beam type, ensuring optimal performance and load-bearing capacity within the reticulated dome structure.

The single-layer reticulated aluminum domes in the design employed two different connection methods, resulting in distinct boundary conditions. First, a fixed support was implemented at the end of the support beams in the outermost ring, effectively constraining all degrees of freedom. This arrangement simulated the connection approach wherein the domes are welded to the tank walls. Subsequently, the sliding supports at the endpoint of the outermost

support beams were converted to the cylindrical coordinate method, limiting all degrees of freedom except for radial translation. This condition replicated the installation scenario where a dome is mounted on a sliding tank. In terms of loads, the domes were subjected to multiple forces. Apart from the static load that accounted for their own weight, live load and wind load were also considered. The live load was further divided into uneven live load and average live load, accounting for variations in applied loads across the dome's surface. These loads were crucial for analyzing the structural response and stability of the domes under operational conditions.

In this study, we utilized the 6061-T6 aluminum alloy as the material for the I-beams in the single-layer reticulated aluminum domes. This particular alloy is renowned for its exceptional strength and lightweight properties, making it highly suitable for constructing domes that necessitate both strength and reduced weight. Note that the study focused solely on the material's characteristics at room temperature, as the impact of varying ambient temperature was not addressed. Table 1 presents the specific values of the material property parameters at room temperature. To assess the compliance of the single-layer reticulated aluminum domes with safety specifications, we subjected them to six load combinations, as outlined in Table 2. These simulations aimed to ascertain whether the domes can withstand the specified load scenarios while maintaining their structural integrity and safety standards.

### 3. Simulation Results and Discussion

The allowable load  $Wa$  encompasses both static and live loads (measured in kPa). It is defined as the maximum load that the single-layer reticulated aluminum domes can safely sustain without compromising their structural integrity and safety standards. The static load accounts for the weight of the domes themselves, while the live load represents additional external forces imposed on the domes during their operation. By considering both static and live loads, the allowable load ensures that the domes can withstand the combined effects of these loads and remain secure and stable. The static load refers to the weight of an object, encompassing the cumulative weight of all its components, such as beams, sheets, battens, gussets, and fasteners. In the case of the designed single-layer reticulated aluminum domes, the total static load, including the weight of the domes and their accessories, amounts to approximately 270,000 N. This value reflects the combined weight of all structural elements and supplementary components in the domes. On the other hand, the live load, also known as the dynamic load, primarily comprises external forces imposed on the single-layer reticulated aluminum domes. It

Table 1  
Relative properties of 6061-T6 aluminum alloy.

Material property	Value
Unit weight	27173.7 N/m <sup>3</sup>
Young's modulus	71000 MPa
Yield stress	280.0 MPa
Ultimate tensile stress	310.0 MPa
Poisson's ratio	0.33

Table 2  
Different load combinations for the designed domes.

Condition	Load combination
Condition 1	Static load
Condition 2	Static load + uneven live load
Condition 3	Static load + average live load
Condition 4	Static load + wind load
Condition 5	Static load + uneven live load + wind load
Condition 6	Static load + average live load + wind load

represents loads that result from external factors, such as foreign objects placed on the domes. The live load can be further categorized into two types, namely, uneven live load and average live load, considering variations in load distribution across the surface of the domes. These load classifications are essential in assessing the structural response and stability of the domes under different operational scenarios.

The analysis process involved several steps. First, the designed dome model was imported into the ANSYS Workbench, which is a finite element analysis software program. Subsequently, material parameters for the various I-structural beams were defined, and the dome model was then meshed, creating a discretized representation for analysis. Once the meshing was complete, boundary conditions were applied to simulate real-world scenarios. According to API Standard 650: Appendix G, specific load requirements were considered. The average live load, mandated to be at least 1 kPa, was uniformly distributed across the entire surface of the domes. Additionally, the uneven live load, stipulated to be at least 0.5 kPa, was applied to half of the dome's area. In terms of wind load, API Standard 650 specified that the minimum wind load corresponds to a static wind pressure of 1.48 kPa, resulting from winds with a speed of 190 km/h. To calculate the actual wind pressure at the site, a factor of  $(155/190)^2$  was applied, resulting in a wind pressure of 0.982 kPa. The wind load was then determined by multiplying this wind pressure by specific pressure coefficients. For the windward direction, 1/4 of the load was obtained by multiplying  $-0.9$  by 0.982, resulting in  $-0.884$  kPa. The middle ward direction accounted for 1/2 of the load and was calculated as  $-0.7$  multiplied by 0.982, yielding  $-0.688$  kPa. Lastly, the leeward direction represented 1/4 of the load and was determined by multiplying  $-0.5$  by 0.982, giving  $-0.491$  kPa. These values reflect the respective wind pressures acting on different sides of the domes during the analysis.

According to the elasticity theory, it is possible to rotate an infinitesimal volume of material within a solid in such a way that only principal stresses remain while all shear stresses become zero. These principal stresses are referred to as the remaining three principal stresses.<sup>(12)</sup> Among them, the maximum principal stress ( $\sigma_1$ ), middle principal stress ( $\sigma_2$ ), and minimum principal stress ( $\sigma_3$ ) are the primary stresses under discussion. Note that the relationship between these three principal stresses is such that  $\sigma_1 > \sigma_2 > \sigma_3$ . These three parameters are then combined with the allowable stress design method to determine whether the material of the domes undergoes deformation or damage. The simulated and analyzed results should encompass the maximum and minimum principal stresses, as well as the overall deformation of the single-layer reticulated aluminum domes being designed. The critical parameter for evaluating whether the dome material has undergone deformation in the design process is the allowable stress ( $\sigma_a$ ). The  $\sigma_a$  for the designed domes can be determined by multiplying the yield stress ( $\sigma_y$ ) of the dome material by a safety factor ( $SF$ ) of 1.65.

$$\sigma_a = \sigma_y / SF \quad (1)$$

For instance, if the yield stress ( $\sigma_y$ ) of the dome material is 280 MPa, then

$$\sigma_a = 280 \text{ MPa} / 1.65 = 169.7 \text{ MPa}. \quad (2)$$

Therefore, if the maximum values of the principal stresses  $\sigma_1$  and  $\sigma_3$  (or the maximum value of the principal stress,  $\sigma_{\max}$ ) of the designed domes exceed 169.7 MPa, the domes, when subjected to different loads, will surpass the yield stress limit of the material used. Consequently, they will not comply with the safety specifications.

Taking into account the static load caused by its own weight, the initial stress experienced by a dome becomes significant. Thus, it is crucial to consider this load during the analysis of initial stress. In the case of analyzing the domes under static load conditions, only the static load was applied. The analysis results for dome 1 are presented in Fig. 2, where Figs. 2(a) to 2(c) illustrate  $\sigma_1$  as 5.20 MPa,  $\sigma_3$  as  $-6.39$  MPa, and the maximum deformation as 3.82 mm, respectively. Similarly, the analysis results for dome 2 are shown in Figs. 3(a) to 3(c), revealing  $\sigma_1$  as 14.97 MPa,  $\sigma_3$  as  $-17.52$  MPa, and the maximum deformation as 5.88 mm, respectively. Importantly, these results are compliant with safety regulations. When subjected to static load conditions, the values of  $\sigma_1$ ,  $\sigma_3$ , and maximum deformation for both designed domes 1 and 2 are relatively small, and the values for dome 2 are larger than those for dome 1.

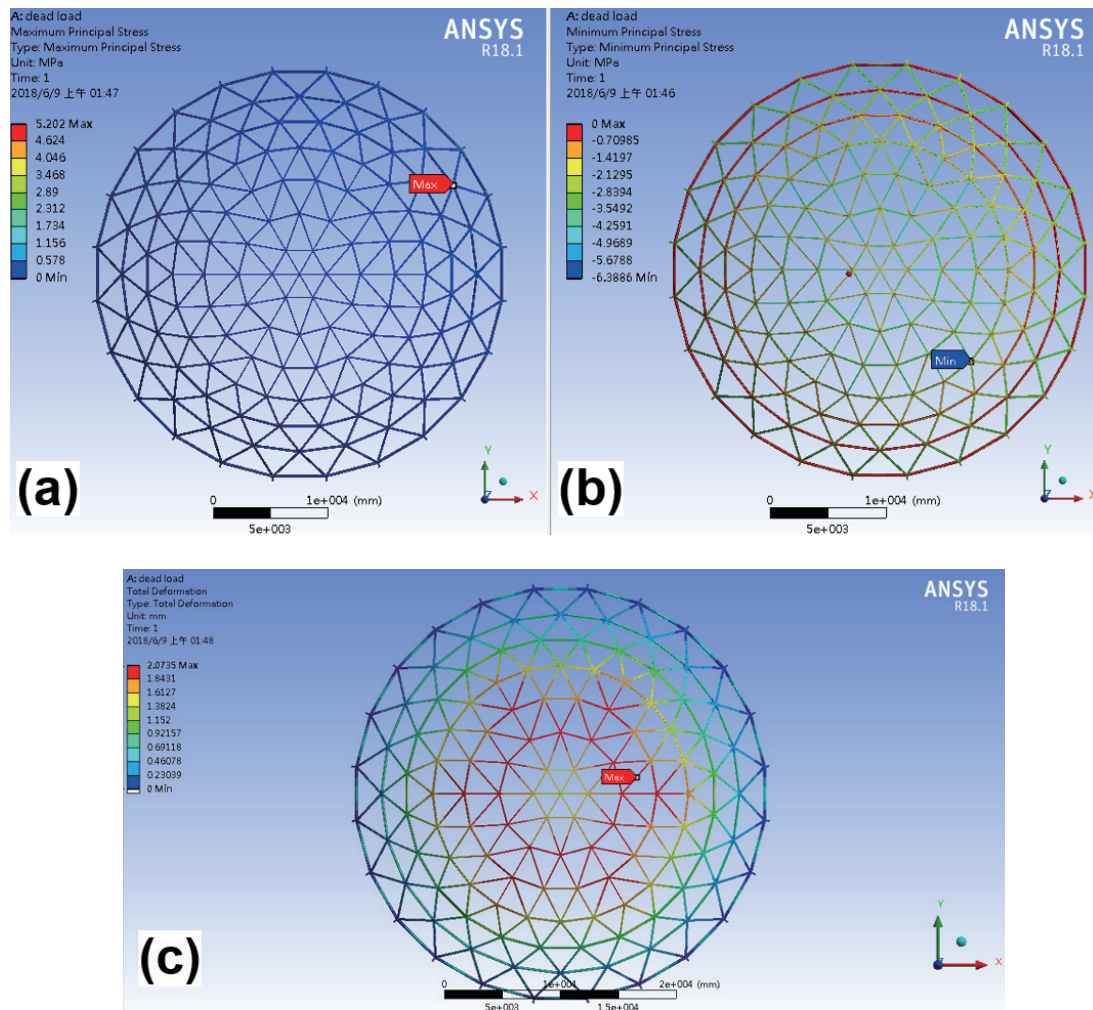


Fig. 2. (Color online) (a) Maximum principal stress, (b) minimum principal stress, and (c) maximum deformation of dome 1 with static load.

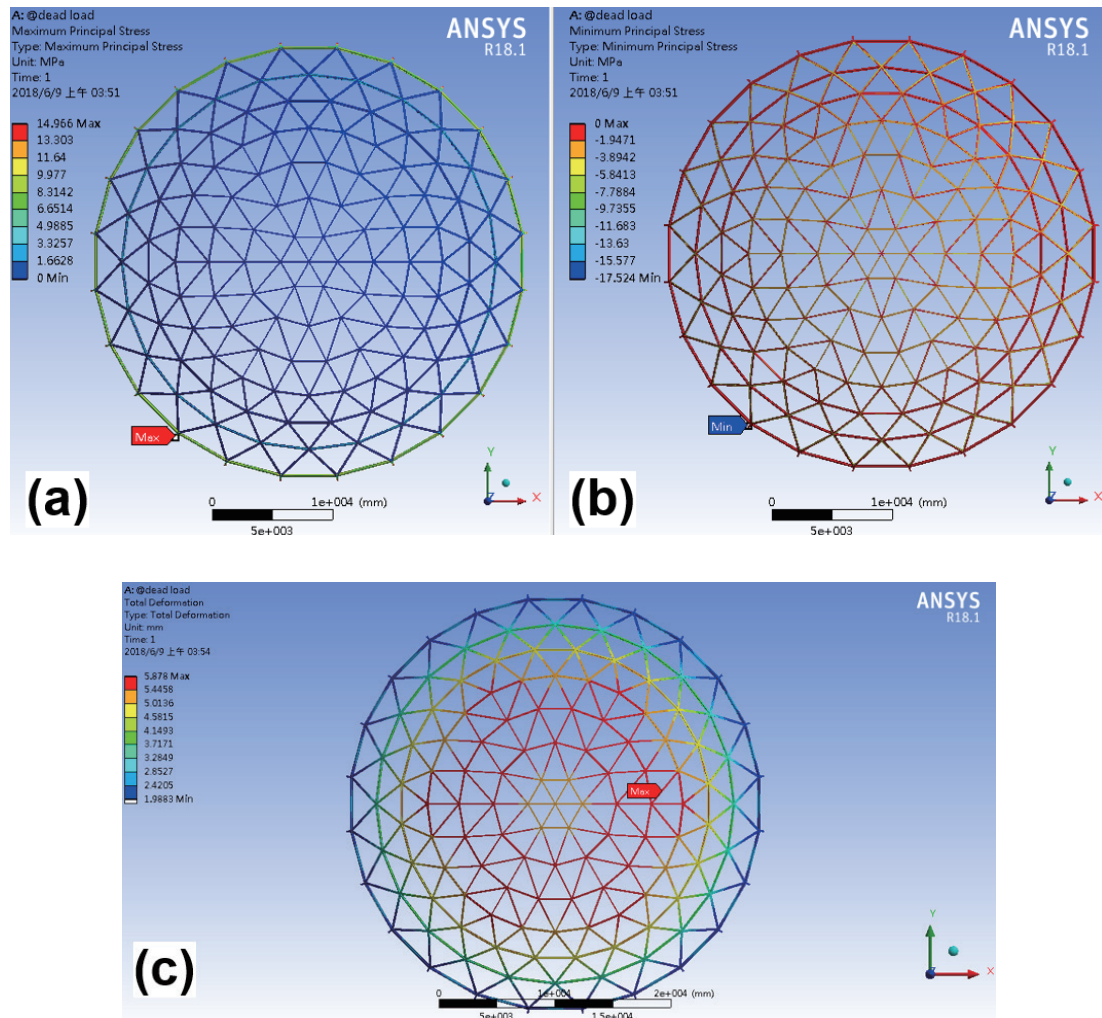


Fig. 3. (Color online) (a) Maximum principal stress, (b) minimum principal stress, and (c) maximum deformation of dome 2 with static load.

In this simulation scenario, we analyzed the effects of both the static and uneven live loads on dome structures. The analysis focused on dome 1, and the results showed that the stress  $\sigma_1$  was 53.01 MPa,  $\sigma_3$  was  $-70.58$  MPa, and the maximum deformation was 12.02 mm, as shown in Figs. 4(a)–4(c), respectively. For dome 2, the analysis results were as follows:  $\sigma_1 = 55.87$  MPa,  $\sigma_3 = -63.37$  MPa, and the maximum deformation was 21.97 mm (note shown here). These values were obtained when both static and uneven live loads were applied simultaneously. Comparing the analysis results of domes 1 and 2, it was evident that the presence of the uneven live load had an impact. In both cases, the stresses  $\sigma_1$ ,  $\sigma_3$ , and the maximum deformation were higher when only the static load was applied. This outcome can be attributed to the effect of the uneven live load on the structures. Importantly, the simulation results demonstrated that the stresses  $\sigma_1$  and  $\sigma_3$ , and the maximum deformation of both designed domes 1 and 2 were still within the limits specified by safety regulations. Thus, these structures complied with the necessary safety standards. Overall, the results indicate that even when both static and uneven live loads are

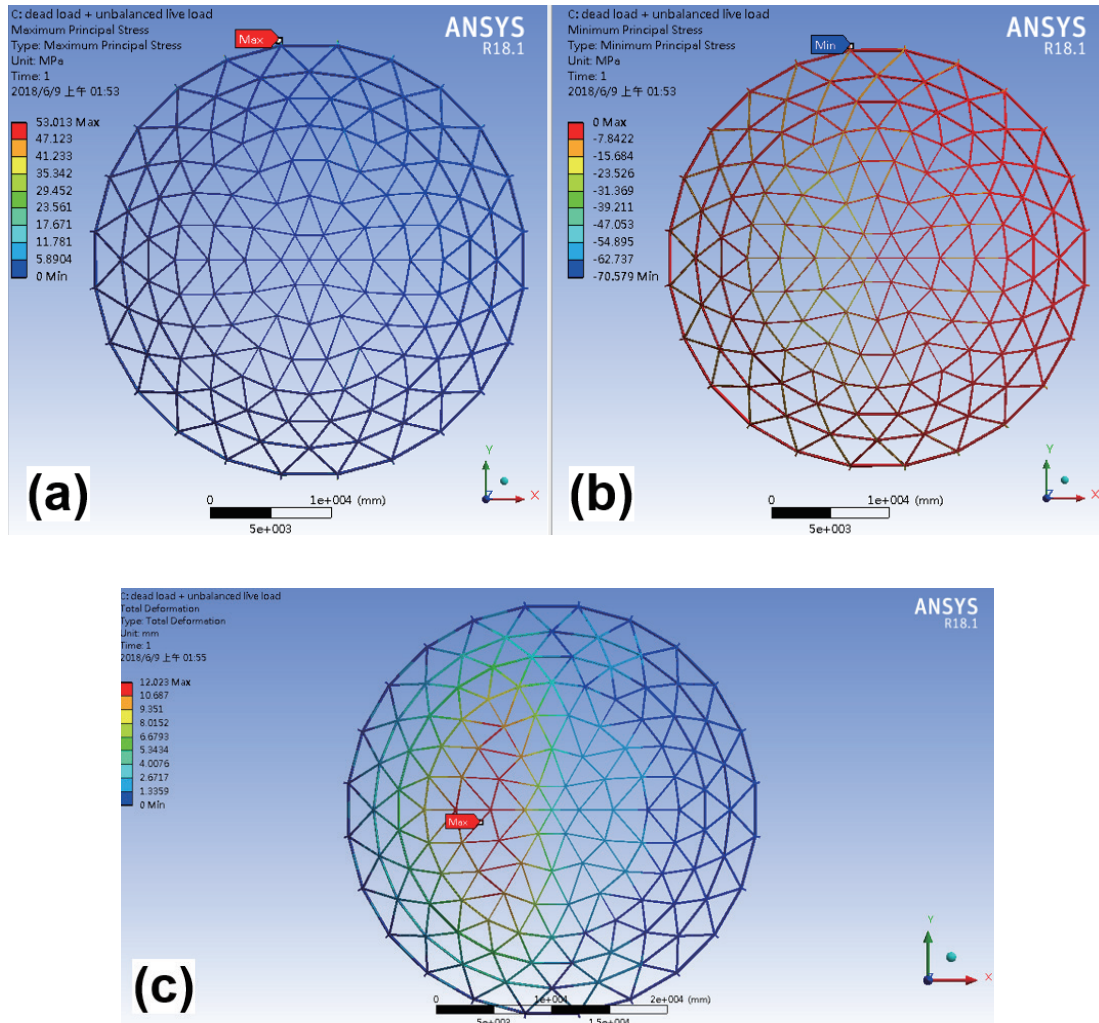


Fig. 4. (Color online) (a) Maximum principal stress, (b) minimum principal stress, and (c) maximum deformation of dome 1 with static load combined with uneven live load.

simultaneously applied to different domes, there are no significant differences in the stresses  $\sigma_1$  and  $\sigma_3$ , and the maximum deformation between the two scenarios.

The simultaneous application of the static and average live loads was performed on the designed domes, and the subsequent analysis focused on dome 1 (analysis results not shown). The analysis of dome 1 revealed that  $\sigma_1$  was 34.38 MPa,  $\sigma_3$  was  $-43.14$  MPa, and the maximum deformation was 15.69 mm. Figure 5 illustrates the analysis results of dome 2;  $\sigma_1$ ,  $\sigma_3$ , and the maximum deformation were 95.92 MPa,  $-112.3$  MPa, and 40.48 mm, respectively. These results were found to comply with safety regulations. When both the static load and average live loads were considered, the  $\sigma_1$ ,  $\sigma_3$ , and maximum deformation values of the designed domes 1 and 2 were significantly greater than when only the static load and the static load combined with the uneven live load were applied. Hence, the average live load is recognized as a crucial factor affecting the safety of the designed dome structures.

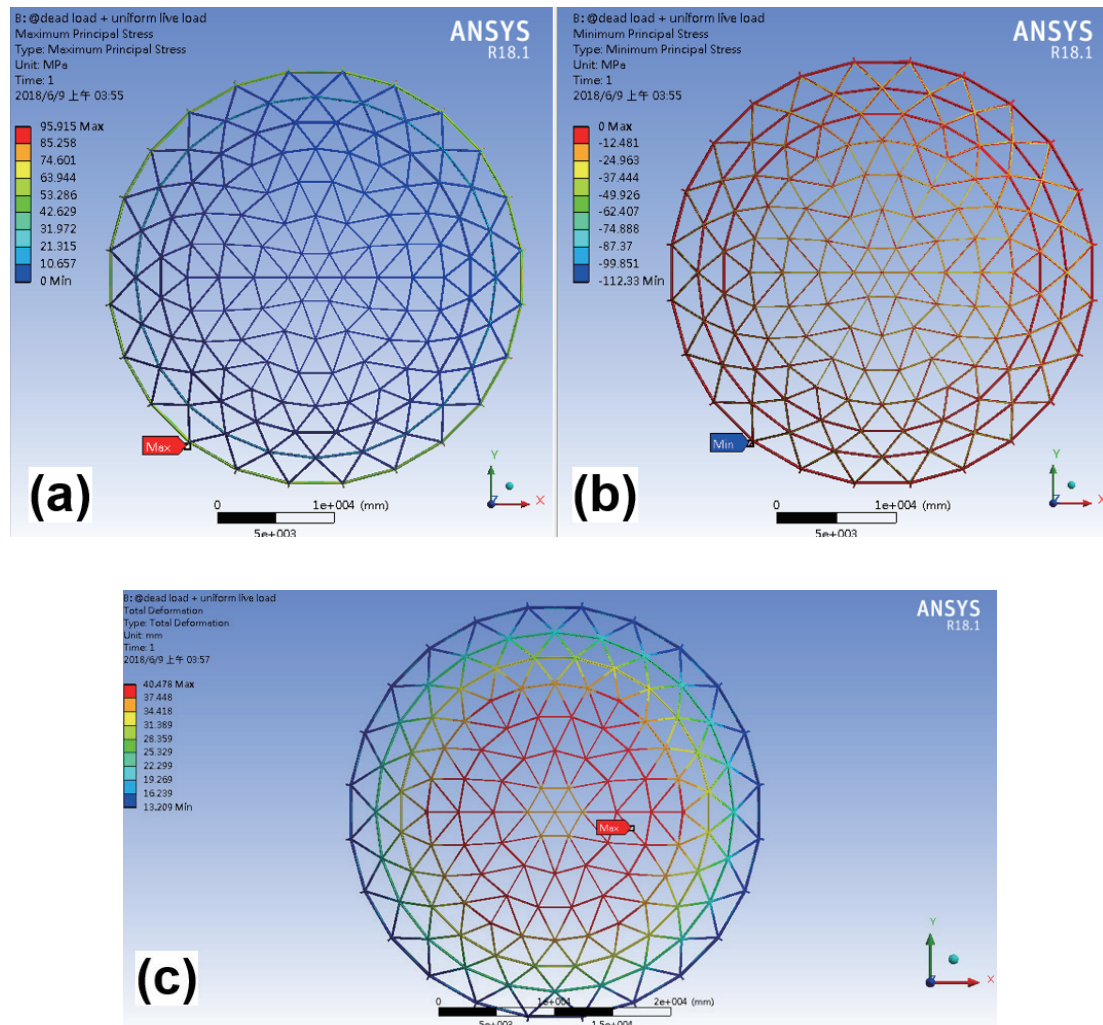


Fig. 5. (Color online) (a) Maximum principal stress, (b) minimum principal stress, and (c) maximum deformation of dome 2 with static load combined with average live load.

Upon applying the different loads to the designed domes, the domes exhibited minimal vibration before settling into deformation in the same direction. As the live load is uniformly distributed and eventually incorporated into the calculation of gravity loads, it can act as a concentrated point load on specific areas. Consequently, when both the static and average live loads are simultaneously applied, the  $\sigma_1$  and  $\sigma_3$ , and maximum deformation values will be larger than when only the static load and the static load combined with the uneven live load were applied. However, it is important to note that the  $\sigma_1$  and  $\sigma_3$ , and maximum deformation values of dome 2 were considerably greater than those of dome 1. This indicates that the structure of dome 1 is more stable and safer than that of dome 2.

The fluctuating wind loads or wind pressures generated by flowing winds are significant factors that impact the stability of long-span domes. In this simulation scenario, both the static and wind loads were applied simultaneously, and the analysis results focused on dome 1, as shown in Fig. 6. The analysis revealed that  $\sigma_1$  was 49.14 MPa,  $\sigma_3$  was -31.88 MPa, and the

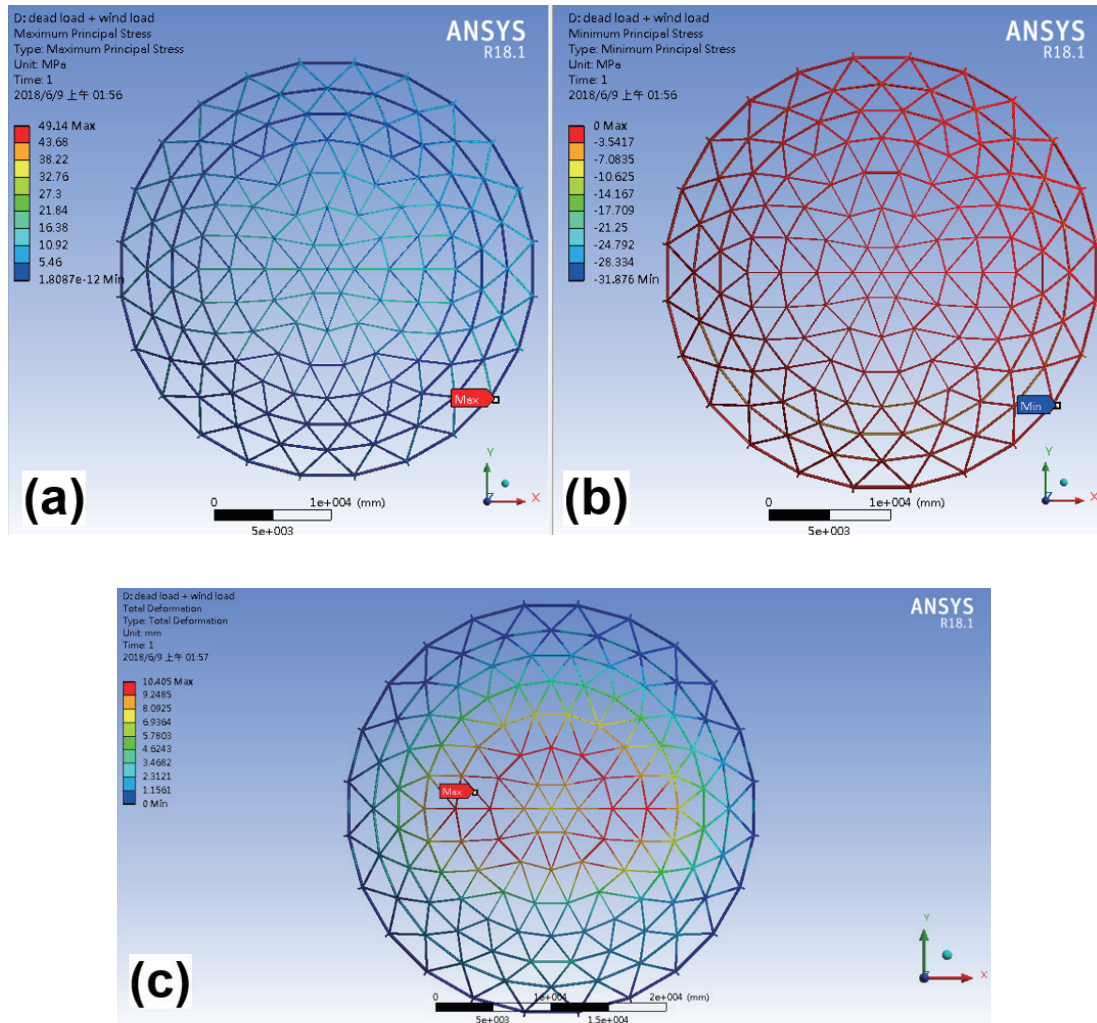


Fig. 6. (Color online) (a) Maximum principal stress, (b) minimum principal stress, and (c) maximum deformation of dome 1 with static load combined with wind load.

maximum deformation was 10.41 mm. For dome 2 (analysis results not shown), the values were as follows:  $\sigma_1 = 68.22$  MPa,  $\sigma_3 = -60.09$  MPa, and the maximum deformation was 21.71 mm. These simulation results for the stresses  $\sigma_1$  and  $\sigma_3$ , and the maximum deformation of both domes 1 and 2 were found to comply with safety regulations. Note that the stresses  $\sigma_1$  and  $\sigma_3$ , and the maximum deformation of dome 2 were significantly larger than those of dome 1, further emphasizing that the structure of dome 1 is more stable and safer than that of dome 2.

When the static load combined with the uneven live load and the wind load were applied to the designed dome simultaneously, the analysis results of dome 1 revealed that  $\sigma_1$  was 65.15 MPa,  $\sigma_3$  was  $-59.71$  MPa, and the maximum deformation was 13.31 mm, as shown in Fig. 7. For dome 2 (analysis not shown), the analysis results showed that  $\sigma_1$  was 57.15 MPa,  $\sigma_3$  was  $-49.90$  MPa, and the maximum deformation was 20.26 mm. Interestingly, when the static, the uneven live, and wind loads were applied simultaneously to both domes 1 and 2, there were no significant differences in  $\sigma_1$  and  $\sigma_3$ , and maximum deformation compared with the case when

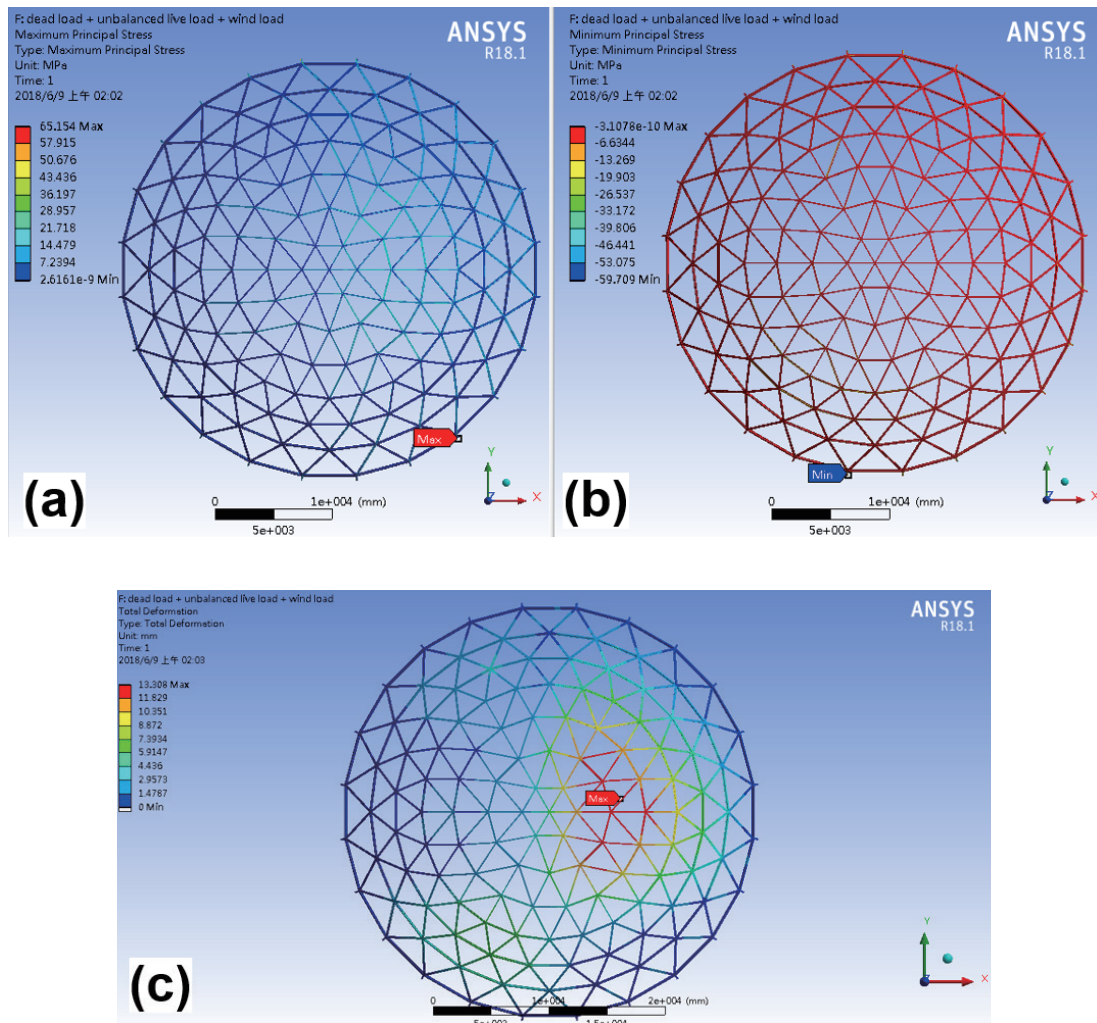


Fig. 7. (Color online) (a) Maximum principal stress, (b) minimum principal stress, and (c) maximum deformation of dome 1 with static load combined with uneven live load and wind load.

only the static and uneven live loads were applied simultaneously.

Under the simulated conditions, the static load combined with the average live load and the wind load were applied simultaneously to the domes. The analysis results of dome 1 (analysis results not shown) indicate that  $\sigma_1$  was 34.29 MPa,  $\sigma_3$  was -54.34 MPa, and the maximum deformation was 10.85 mm. For dome 2, as shown in Fig. 8, the values were as follows:  $\sigma_1 = 63.01$  MPa,  $\sigma_3 = -71.58$  MPa, and the maximum deformation was 21.78 mm. When the static, average live, and wind loads were applied simultaneously, dome 1 exhibited negligible changes in the values of  $\sigma_1$ ,  $\sigma_3$ , and maximum deformation compared with the case where only the static and average live loads were applied. However, in the case of dome 2, the  $\sigma_1$ ,  $\sigma_3$ , and maximum deformation were significantly reduced when the static, average live, and wind loads were considered together, as opposed to when only the static and average live loads were applied.

One possible explanation for this phenomenon is that the direction of the forces generated by

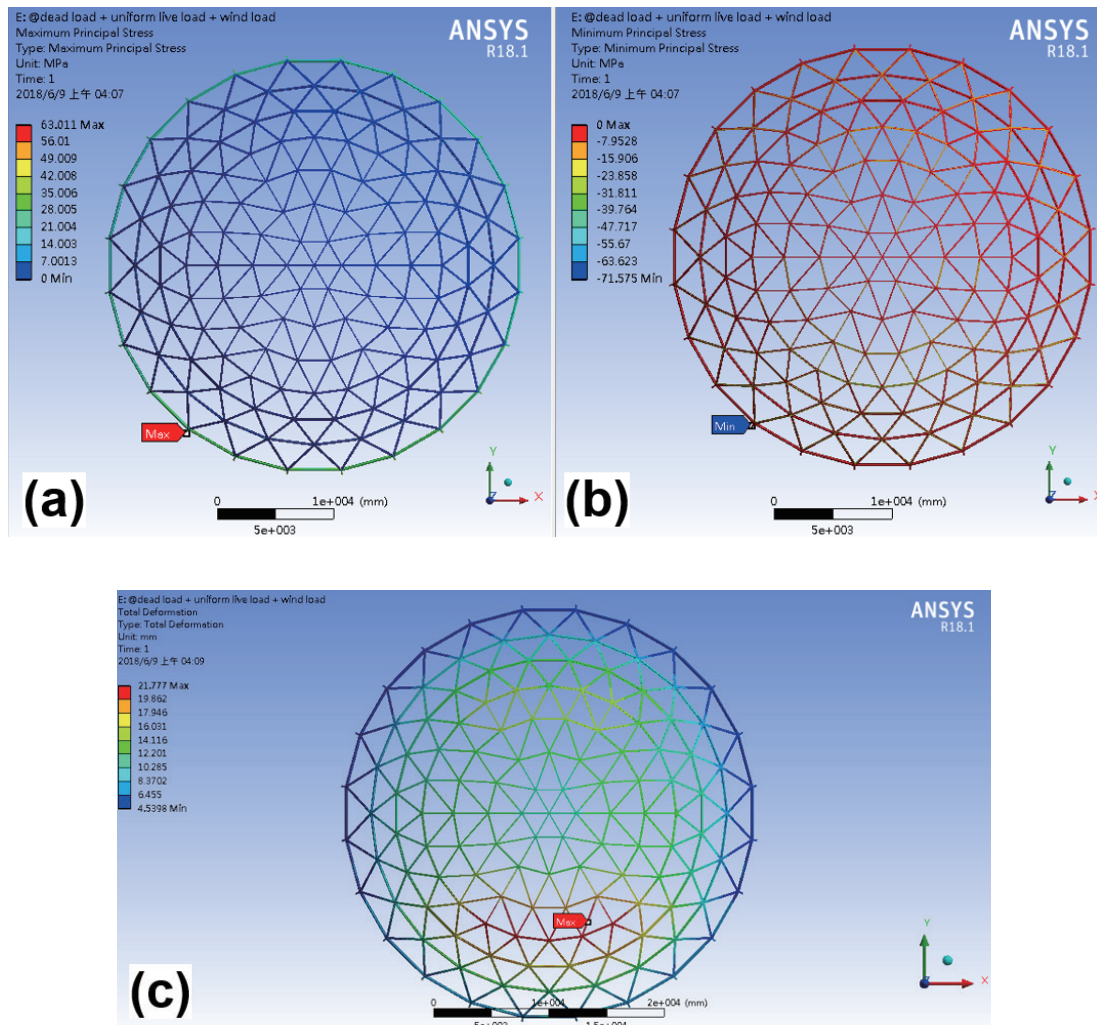


Fig. 8. (Color online) (a) Maximum principal stress, (b) minimum principal stress, and (c) maximum deformation of dome 1 with static load combined with average live load and wind load.

the wind differs from that of the forces generated by the static and average live loads (especially the average live load). As a result, the stresses induced by the average live and wind loads partially offset each other, leading to a reduction in the response of the designed domes to the average live load. Consequently,  $\sigma_1$ ,  $\sigma_3$ , and the maximum deformation become smaller in the presence of all three loads. These results once again confirm that the static, uneven live, and wind loads are not the primary factors affecting the safety of the designed domes. Instead, the average live load remains the most crucial factor in determining the structural safety of the domes.

On the basis of our simulation results, none of the single-layer mesh aluminum domes designed in this study demonstrated any permanent deformation. This outcome serves as compelling evidence that the designed mesh aluminum domes successfully meet the required safety specifications. Moreover, these designed domes effectively distribute the loads, thereby

minimizing the concentration of forces at individual nodes. This means that the various loads are uniformly distributed to all nodes and tubes in accordance with their respective load distribution regions. Consequently, the domes ensure an even distribution of stress throughout the structure. To comprehensively analyze the structural performance, we have consolidated all the relevant data in Tables 3 and 4. These tables provide a comprehensive overview of the maximum normal stresses and deformations under different load conditions. By examining their values, we gain valuable insights into the structural behavior of the mesh aluminum domes and can evaluate their performance with greater precision.

The analysis reveals that, in the majority of load conditions, dome 1 exhibits a smaller maximum normal stress than dome 2. Additionally, all maximum deformations observed in dome 1 are significantly smaller than those observed in dome 2. These findings, as presented in Tables 4 and 5, highlight the structural performance differences between the two domes. Furthermore, the combined static and average live loads lead to dome 2 experiencing the highest levels of stress and deformation. Therefore, it is crucial to give special consideration to this particular load condition during the dome's design phase. However, it is important to note that even when subjected to the six different loads, both domes exhibit maximum stresses that are considerably lower than the maximum stress tolerance of the material used (6061-T6 aluminum alloy). Consequently, even with a maximum deformation of 40.48 mm caused by the static load combined with the average live load, the domes will not undergo permanent deformation. These observations provide reassurance regarding the structural integrity of the designed domes and validate their compliance with safety standards.

#### 4. Conclusions

Table 3

Analysis results of the maximum normal stress of the designed domes for various load combinations.

Load combinations	Maximum normal stress $\sigma_{max}$ (MPa)	
	Dome 1	Dome 2
Static load	6.39	17.52
Static load + uneven live load	70.58	63.37
Static load + average live load	43.14	122.3
Static load + wind load	49.14	68.22
Static load + uneven live load + wind load	65.15	57.15
Static load + average live load + wind load	53.34	71.58

Table 4

Analysis results of the maximum deformation of the designed domes for various load combinations.

Load combinations	Maximum deformation (mm)	
	Dome 1	Dome 2
Static load	3.82	5.88
Static load + uneven live load	12.02	21.97
Static load + average live load	15.69	40.48
Static load + wind load	10.41	21.71
Static load + uneven live load + wind load	13.31	20.26
Static load + average live load + wind load	10.85	21.78

In this study, simulation results indicated that dome 1 experienced a maximum stress of 70.58 MPa under static load combined with uneven live load, and a maximum deformation of 15.69 mm under static load combined with average live load. For dome 2, both the maximum stress (122.3 MPa) and maximum deformation (40.48 mm) occurred under static load combined with average live load. Throughout the six load conditions, most of the maximum normal stresses were lower in dome 1 than in dome 2. However, when static load was combined with uneven live load or combined with uneven live load and wind load, the maximum normal stresses in dome 1 surpassed those in dome 2. Nevertheless, under all six load conditions, dome 1 exhibited smaller maximum deformations than dome 2. When the static, average live, and wind loads were applied simultaneously, dome 1 displayed negligible changes in  $\sigma_1$ ,  $\sigma_3$ , and maximum deformation compared with the case where only the static and average live loads were considered. Conversely, dome 2 experienced significant reductions in  $\sigma_1$ ,  $\sigma_3$ , and maximum deformation when the static, average live, and wind loads were applied, as opposed to when only the static and average live loads were applied. This phenomenon can possibly be explained by the different forces generated by the wind compared with the forces generated by the static and average live loads, particularly the average live load.

### Acknowledgments

This work was supported by the Foreign Cooperation Project of Fujian Provincial Department of Science and Technology (Grant No. 2020I0022), MOST 109-2221-E-390-023, MOST 110-2622-E-390-002, and MOST 110-2221-E-390-020.

### References

- 1 S. Kato, J. M. Kim, and M. C. Cheong: *Eng. Struct.* **25** (2003) 1265.
- 2 A. Chandiwala: *Int. J. Res. Eng. Technol.* **3** (2014) 35.
- 3 F. Fan, D. Wang, X. Zhi, and S. Shen: *Trans. Tianjin University* **14** (2008) 545.
- 4 F. Fan, Z. Cao, and S. Shen: *Thin-Walled Struct.* **48** (2010) 827.
- 5 G. Nie, X. Zhi, F. Fan, and J. F. Dai: *J. Constr. Steel. Res.* **100** (2014) 176.
- 6 J. Ma, F. Fan, C. Wu, and X. Zhi: *Thin-Walled Struct.* **96** (2015) 130.
- 7 Y. Jihong and Q. Nian: *J. Constr. Steel. Res.* **128** (2017) 721.
- 8 G. Nie and K. Liu: *Shock Vib.* **2018** (2018) 6041878.
- 9 C. Zhao, J. Ma, S. Du, Y. Gu, and Y. Zhou: *Mater. Technol.* **53** (2019) 811.
- 10 Y. Uematsu, M. Yamada, A. Inoue, and T. Hongo: *J. Wind. Eng. Ind. Aerodyn.* **66** (1997) 227.
- 11 C. Wang and S. Shen: *Adv. Steel Struct.* **1** (1999) 201.
- 12 ANSYS 15.0. *Mechanical User's Guide: Material Models Used in Explicit Dynamics Analysis*, 2013.